

# Laser-driven proton scaling laws and new paths towards energy increase

J. FUCHS<sup>1,2\*</sup>, P. ANTICI<sup>1,2,3,4</sup>, E. D'HUMIÈRES<sup>5</sup>, E. LEFEBVRE<sup>5</sup>, M. BORGHESI<sup>6</sup>, E. BRAMBRINK<sup>1</sup>, C. A. CECCHETTI<sup>6</sup>, M. KALUZA<sup>7</sup>, V. MALKA<sup>8</sup>, M. MANCLOSSI<sup>8,9</sup>, S. MEYRONEINC<sup>10</sup>, P. MORA<sup>11</sup>, J. SCHREIBER<sup>7</sup>, T. TONCIAN<sup>12</sup>, H. PÉPIN<sup>3</sup> AND P. AUDEBERT<sup>1</sup>

<sup>1</sup>Laboratoire pour l'Utilisation des Lasers Intenses, UMR 7605 CNRS-CEA-École Polytechnique-Université Paris VI, 91128 Palaiseau, France

<sup>2</sup>Physics Department, MS-220, University of Nevada, Reno, Nevada 89557, USA

<sup>3</sup>INRS-ÉMT, 1650 bd. L. Boulet, J3X1S2 Varennes, Québec, Canada

<sup>4</sup>Dipartimento di Energetica, Università di Roma 'La Sapienza', Via Scarpa 14-16, 00161 Roma, Italy

<sup>5</sup>Département de Physique Théorique et Appliquée, CEA-DIF, BP 12, 91680 Bruyères-le-Châtel, France

<sup>6</sup>School of Mathematics and Physics, The Queen's University, Belfast BT7 1NN, UK

<sup>7</sup>Max-Planck-Institut für Quantenoptik, 85748 Garching, Germany

<sup>8</sup>Laboratoire d'Optique Appliquée –ENSTA, UMR 7639, CNRS, Ecole Polytechnique, 91761 Palaiseau, France

<sup>9</sup>Dipartimento di Fisica 'G. Occhialini' and INFN, Università di Milano-Bicocca, 20126 Milano, Italy

<sup>10</sup>Centre de Protonthérapie d'Orsay, BP 65, 91402 Orsay, France

<sup>11</sup>Centre de Physique Théorique, UMR 7644 CNRS-Ecole Polytechnique, 91128 Palaiseau, France

<sup>12</sup>Institut für Laser und Plasmaphysik, Heinrich-Heine-Universität, 40225 Düsseldorf, Germany

\*e-mail: julien.fuchs@polytechnique.fr

Published online: 25 December 2005; doi:10.1038/nphys199

The past few years have seen remarkable progress in the development of laser-based particle accelerators. The ability to produce ultrabright beams of multi-megaelectronvolt protons routinely has many potential uses from engineering to medicine, but for this potential to be realized substantial improvements in the performances of these devices must be made. Here we show that in the laser-driven accelerator that has been demonstrated experimentally to produce the highest energy protons, scaling laws derived from fluid models and supported by numerical simulations can be used to accurately describe the acceleration of proton beams for a large range of laser and target parameters. This enables us to evaluate the laser parameters needed to produce high-energy and high-quality proton beams of interest for radiography of dense objects or proton therapy of deep-seated tumours.

**E**nergetic proton beams with high beam quality have been produced in the last five years from thin metallic foils (usually aluminium) irradiated by ultraintense short laser pulses<sup>1–3</sup>. Protons accelerated from solids originate primarily from contaminant layers of water vapour and hydrocarbons on the target surface<sup>4</sup>.

These proton beams are extremely laminar<sup>5,6</sup>, collimated ( $\sim 15^\circ$  half-angle with a divergence decreasing with the beam energy) with a smooth angular distribution<sup>7</sup> and have a duration at the source of the order of a picosecond. Owing to these qualities, these beams are already being considered or applied in high-resolution charged-particle radiography<sup>8</sup>, or for the production of high-energy-density matter of interest for astrophysics<sup>9</sup>; they could also lead to high-brightness injectors for accelerators<sup>5</sup> or sources for proton therapy<sup>10–12</sup> or radioisotope production<sup>13</sup>.

However, these present-day sources are not yet optimized for the intended applications. The determination of the scaling laws discussed here is a necessary step to achieve this optimization. Several scaling studies have already been carried out on different facilities (from small table-top lasers to single-pulse large laser facilities)<sup>14–21</sup>. However, as they cannot be fully compared owing to the different sets of parameters used, no clear picture has yet emerged of the relative importance of the various target (thickness) and laser parameters (pulse energy, pulse duration, peak intensity and focal spot size).

Here we present the results of a series of experiments on aluminium foils, measuring the proton-beam maximum energy

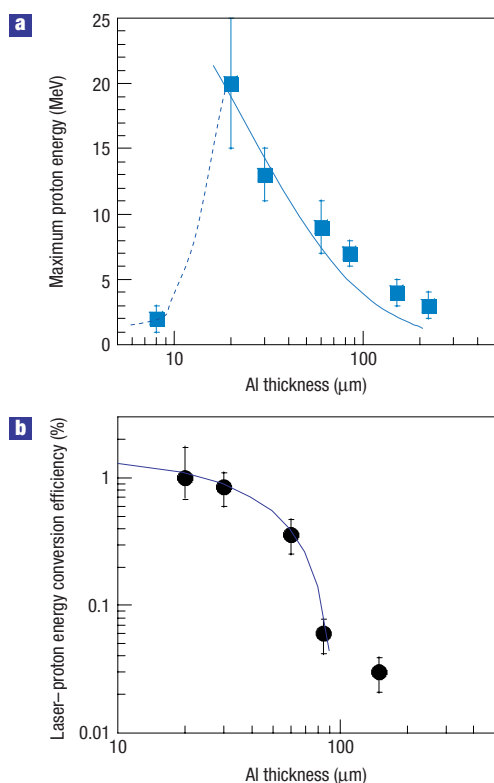


**Figure 1** Thinner solid targets improve the maximum energy of laser-accelerated protons as well as the laser–proton energy conversion efficiency. **a**, Maximum proton energy, and **b**, laser–proton energy conversion (calculated for protons with energy  $> 4$  MeV) for similar laser conditions ( $\tau_{\text{laser}} = 320$  fs and  $I \sim 4 \times 10^{19}$  W cm $^{-2}$ ) and various Al foil thicknesses. Data points represent experimental data and solid lines calculations using the fluid model with the same laser parameters. The dashed line is a guide for the eye. Error bars on the proton energy represent the shot-to-shot fluctuation cumulated with the simulated measurement uncertainty in the detector. Error bars on the energy conversion efficiency are standard deviation, and take into account the maximum energy error bar, the error in the laser energy and the uncertainty in the calibration of the detector that induces uncertainties in the absolute proton number.

and energy-conversion efficiency as a function of varying laser and target parameters. The experimental scaling laws compare favourably with the prediction of a simple fluid-based model of proton acceleration. Two-dimensional particle-in-cell (PIC) simulations illuminate and support the successful use of the fluid model. The fluid model emerges as a helpful predictive tool for high-energy and high-quality proton-beam production of interest, for example, for radiography of dense objects or for proton therapy.

Finally, we discuss alternative paths for the central task of increasing the maximum energy of the proton beam, with particular attention to a new regime using volumetric heating of ultrathin targets by ultrahigh-temporal-contrast laser pulses.

## ACCELERATION MECHANISMS

Up to the maximum laser intensities currently achievable, the basic mechanism involved in the production of these proton beams is electrostatic acceleration of protons at the target rear (non-irradiated) surface<sup>22–24</sup>. At higher intensities, numerical simulations (discussed below) show that this mechanism is still effective. The

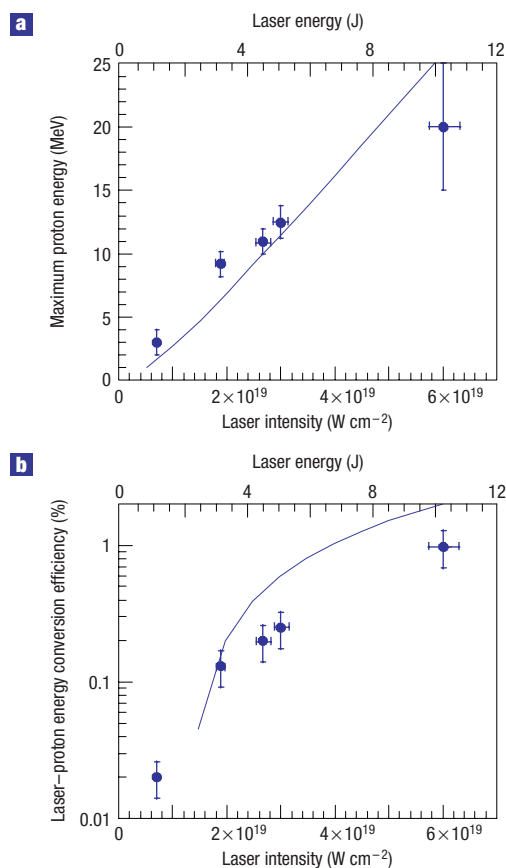


**Figure 2** The laser-accelerated proton maximum energy and conversion efficiency increase with laser pulse energy. **a**, Maximum energy of the proton beam and **b**, laser–proton energy conversion efficiency (for protons with energy  $> 4$  MeV) as a function of the laser intensity (bottom axis) and the laser energy in the focal spot (top axis). The laser pulse duration is constant at 320 fs. The lines in **a** and **b** are calculations using the fluid model with the actual laser parameters. Error bars on the laser energy are the standard deviation of the uncertainties in the calorimeter calibration. Vertical error bars are estimated similarly to Fig. 1.

proton acceleration is achieved by charge-separation electric fields induced by the laser-accelerated electrons produced at the front surface going through the target and emerging from the rear.

For completeness, we mention two other ways in which fast protons may be produced at sufficiently high intensities, but whose scaling will not be discussed, failing any experimental testing of the concepts. First, at higher laser intensities, that is, above  $\sim 10^{21}$  W cm $^{-2}$ , numerical simulations seem to indicate that laser-induced ion shocks could also accelerate protons to high energies<sup>25</sup>. However, simulations also show that fewer protons are produced by this method than by acceleration at the target rear surface, with lower beam quality and with large fluctuations in the maximum beam energy owing to the instabilities to which this mechanism is linked<sup>26</sup>. Second, also according to simulations, for extreme intensities approaching  $10^{23}$  W cm $^{-2}$ , the interaction shows a continuous transition from the rear-surface acceleration/shock acceleration regimes to a regime where the radiation pressure of the electromagnetic wave is directly converted into ion energy by the space-charge force related to the displacement of the electrons in a thin foil<sup>27</sup>. In this regime the proton energies could reach giga-electronvolts and the efficiency of the laser energy conversion into fast ion energy could be much higher than projected from

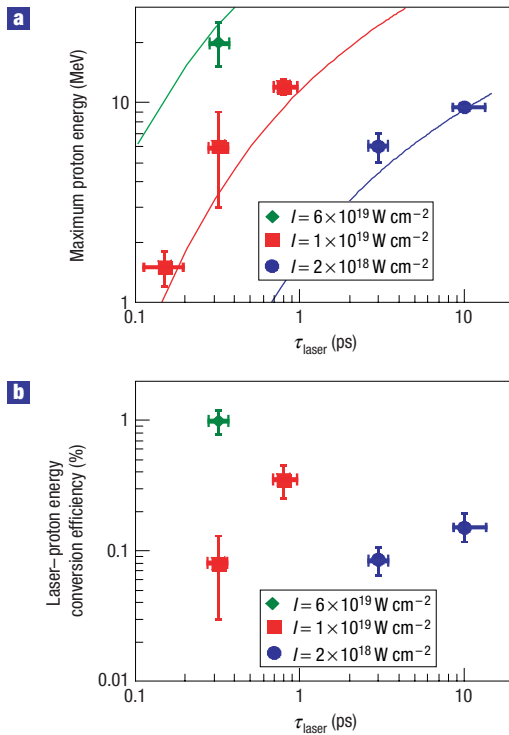


**Figure 3** Longer pulses improve the laser-accelerated proton maximum as well as the energy conversion efficiency. **a**, Maximum energy of the proton beam and **b**, laser–proton energy conversion efficiency (for protons with energy  $> 4$  MeV) as a function of the laser pulse duration for three different laser intensities; the laser energy is increased with the laser pulse duration to keep the laser intensity constant for each group of points. The lines are calculations for each intensity using the fluid model. Error bars on the laser pulse duration represent the shot-to-shot fluctuation combined with the estimated error linked to assuming different pulse shapes for the pulse-duration retrieval. Vertical error bars are estimated similarly to Fig. 1.

what is presently known. This transition, however, remains to be observed experimentally.

As applications require robustness and high beam quality, in this work we will concentrate on the rear-surface mechanism that has been experimentally proven in several facilities and that has been shown to satisfy these two criteria.

## EXPERIMENTAL RESULTS AND MODELLING

In the series of experiments reported here, we have measured the proton spectra accelerated from laser-irradiated solid aluminium targets while varying only one parameter at a time, either laser intensity ( $I$ ), laser energy ( $E$ ), laser pulse duration ( $\tau_{\text{laser}}$ ) or target thickness ( $d$ ). Other conductor targets (for example, gold) give similar proton-beam results to those using aluminium. Insulator targets, on the other hand, show unsatisfactory filamentary proton beams<sup>7</sup>. Hence aluminium targets are all that are studied here. We have compared simultaneously all the obtained scalings with a simple self-similar, isothermal, time-limited fluid model<sup>28</sup> using a single free parameter, the effective acceleration time (or limit time)  $t_{\text{acc}}$ . As we will see below,  $t_{\text{acc}} \sim 1.3\tau_{\text{laser}}$  matches well with all the scaling results that we obtained.

The energy spectrum observed both in experiments and in simulations can be approximated by a quasithermal distribution with a sharp cutoff at a maximum energy. Typical spectra observed in the experimental conditions reported here can be seen in refs 21,24.

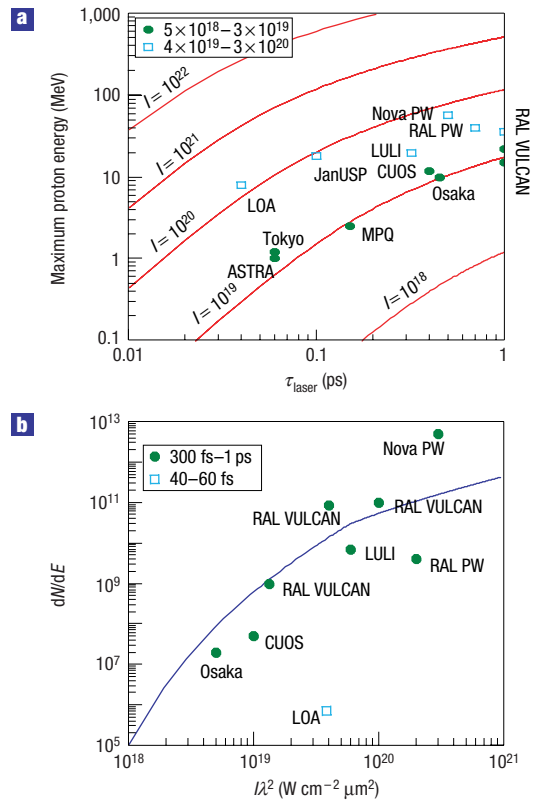


**Figure 4** Comparison between fluid-model predictions and previously published data. **a**, Maximum proton energy as a function of laser pulse duration. Circles and squares are experimental data for the two intensity ranges; the intensities are in units of  $\text{W cm}^{-2}$ . Lines represent calculations for various laser intensities, as indicated in units of  $\text{W cm}^{-2}$ , using the fluid model assuming 20- $\mu\text{m}$ -thick targets and a 10  $\mu\text{m}$  FWHM laser spot size. **b**, Number of protons in a 1 MeV bin around 10 MeV as a function of laser intensity multiplied by the laser wavelength squared. The last parameter is chosen as it governs the hot electron temperature  $T_p$ . Circles and squares are experimental data for the two laser-pulse-duration ranges shown. The line is given by the fluid model assuming 20- $\mu\text{m}$ -thick targets, a 10  $\mu\text{m}$  FWHM laser spot size and a 0.5 ps laser pulse duration. References are as follows: LOA<sup>12</sup>, JanUSP<sup>20</sup>, RAL PW<sup>46</sup>, Nova PW<sup>2</sup>, RAL VULCAN<sup>16,17</sup>, Osaka<sup>47</sup>, CUOS<sup>48</sup>, MPQ<sup>21</sup>, Tokyo<sup>49</sup>, ASTRA<sup>18</sup>. LULI represents the data presented in this article (see Fig. 2).

The maximum (cutoff) energy that can be gained by the accelerated ions based on the simple self-similar, isothermal, fluid model (for example, equation (10) of ref. 28) is given by

$$E_{\text{max}} = 2T_{\text{hot}}[\ln(t_p + (t_p^2 + 1)^{1/2})]^2, \quad (1)$$

where  $t_p = \omega_{\text{pi}} t_{\text{acc}} / (2\exp^{1/2})$  is the normalized acceleration time, normalized using the ion (of charge number  $Z_i$  and mass  $m_i$ ; for protons  $Z_i = 1$ ,  $m_i = m_p$ ) plasma frequency  $\omega_{\text{pi}} = [(Z_i \times e^2 \times n_{e0}) / (m_i \times \epsilon_0)]^{1/2}$ , with  $e$  the electron charge,  $\epsilon$  the electric permittivity, and  $T_{\text{hot}}$  and  $n_{e0}$  the temperature and density of the hot electrons that drive the rear-surface expansion. This model updates previous models of freely expanding plasma<sup>29</sup> with a steady electron temperature (and thus unlimited acceleration) to the case of a sudden burst of energetic electrons. As our simple model cannot take into account the progressive transfer of energy from the fast electrons to the ions and the decrease of the accelerating charge separation field, we use the crude approximation of simply fixing the acceleration time in a way dictated by the laser pulse length. We

**Table 1** Comparison between maximum proton energy observed in two-dimensional PIC simulations and that calculated by the fluid model. The comparison is made mainly at 36-fs laser pulse duration for practical computational time limitations.

$I$ ( $\text{W cm}^{-2}$ )	$\tau_{\text{laser}}$ (fs)	Focal spot FWHM ( $\mu\text{m}$ )	Target thickness ( $\mu\text{m}$ )	Proton $E_{\text{max}}$ from PIC (MeV)	Proton $E_{\text{max}}$ from model (MeV)
$1 \times 10^{22}$	36	6	2	319	368
$2 \times 10^{21}$	36	6	2	111	108
$1 \times 10^{21}$	36	6	2	60	63
$3 \times 10^{20}$	36	6	1	37	27
$3 \times 10^{20}$	150	6	4	72	82
$3 \times 10^{19}$	320	6	19	16	13

will see below that, considering the results of the PIC simulations, although not physically accurate, this approximation works well.

As in most of the experiments, a preformed plasma (preplasma) was present in front of the target owing to long-duration, low-level laser energy reaching the target before the main pulse. Following the irradiation by the main pulse, the temperature of the fast electrons produced in this preplasma  $T_{\text{hot}}$  is found numerically and experimentally to be given by the laser ponderomotive potential  $T_p = m_e c^2 [(1 + I \lambda_{\text{um}}^2 / 1.37 \times 10^{18})^{1/2} - 1]$ , where  $m_e$  is the electron mass,  $c$  is the velocity of light,  $I$  is the laser power density ('intensity') in  $\text{W cm}^{-2}$  and  $\lambda_{\text{um}}$  is the laser wavelength in micrometres<sup>30,31</sup>. We estimate  $n_{e0}$  by considering that the electrons accelerated at the target front surface are ballistically sprayed into the target. The total number of electrons accelerated into the target is  $N_e = fE/T_p$ , where  $f$  is the fraction of laser light that is absorbed into the preplasma as fast electrons. This fraction  $f$  has been found to depend on the laser incident intensity as follows:  $f = 1.2 \times 10^{-15} I^{0.74} (\text{W cm}^{-2})$  with a maximum of 0.5 (refs 32,33). As the  $N_e$  electrons are accelerated over the laser pulse duration and spread over the surface of the sheath  $S_{\text{sheath}}$ , we have  $n_{e0} = N_e / (c \tau_{\text{laser}} S_{\text{sheath}})$  with  $S_{\text{sheath}} = \pi(r_0 + d \times \tan \theta)^2$ . The latter depends on the half-angle divergence ( $\theta \sim 25^\circ$ ) of the hot electron inside the target<sup>7</sup>, the target thickness  $d$  and the initial radius  $r_0$  of the zone over which the electron are accelerated at the target front surface, that is, the laser spot. Note that the values of the sheath extension obtained with this model (for example,  $\sim 25 \mu\text{m}$  for a  $18\text{-}\mu\text{m}$ -thick target) are in good agreement with direct measurements of the sheath size (see Figure 2c of ref. 5). Finally, an effective 'acceleration time',  $t_{\text{acc}}$ , has to be defined. Otherwise, because of its isothermal hypothesis (that is, no energy depletion of the electrons), the fluid model of ref. 28 would predict endless proton acceleration.

The fluid model also gives the number of accelerated protons per unit energy:

$$dN/dE = [n_{e0} c_s t_{\text{acc}} S_{\text{sheath}} / (2ET_{\text{hot}})^{1/2}] \exp(-(2E/T_{\text{hot}})^{1/2}), \quad (2)$$

where  $c_s = (Z_i \times T_{\text{hot}}/m_i)^{1/2}$  is the sound speed.

We can thus compare the experimental value of the laser–proton energy conversion efficiency with the one given by the model. Both are obtained by integrating the spectrum between a fixed minimal energy, here chosen to be 4 MeV, and the maximum cutoff energy, and by dividing this number by the laser initial energy.

As shown in Fig. 1, a decrease in target thickness results in an increase in the maximum proton energy and in the energy conversion efficiency. However, if the target is too thin ( $\leq 8 \mu\text{m}$  for the parameters of Fig. 1), protons are not accelerated to high energies. This is consistent with the fact that, for targets that are too thin, the rear surface is massively perturbed by the shock wave launched  $\sim 1$  ns before the main pulse by the laser amplified spontaneous emission (ASE)<sup>21</sup>. For the thicker targets of interest here, this slow shock-wave preheating does not have

the time to reach the rear surface before the formation of the hot electron sheath. Using equation (1) to compute the maximum proton energy and equation (2) to compute the laser–proton energy conversion efficiency, we find a good agreement with the experimental data, taking, as mentioned above,  $t_{\text{acc}} = 1.3 \times \tau_{\text{laser}}$ . This is shown in Fig. 1.

Good agreement is also found between the isothermal fluid model and the measurements when studying the dependence of the proton-beam energy characteristics with laser energy (keeping the pulse duration constant) as shown in Fig. 2, or laser pulse duration (keeping the laser intensity constant) as shown in Fig. 3. For both of these, the targets are  $25\text{-}\mu\text{m}$ -thick Al foils.

Figure 2b shows that the energy conversion efficiency increases more with laser energy than the laser energy does when the pulse duration is kept constant. This is due to the fact that when one increases the laser energy, the proton spectrum extends to higher energies and that the number of particles also scales up. This means, for instance, that one would obtain more energy in the proton beam with a single shot at 10 J rather than cumulating 10 shots at 1 J.

Regarding Fig. 3b, we find that the model gives, in the case of long laser pulses, lower energy-conversion efficiency compared with the measured ones. As this discrepancy cannot be due to errors in the maximum proton energy, which is well modelled, it must be due to the spectral slope being underestimated by the model, perhaps owing to circulation effects<sup>20</sup> that become important at long pulse durations.

We also find the same good agreement between experimental data and the model when we vary the pulse duration while keeping the laser energy constant; here the dependence of the maximum proton energy on the laser pulse duration is rather weak.

Note that in a complementary regime of shorter pulses, 55–400 fs, the dependence of the proton maximum energy with laser energy and pulse duration has been explored<sup>19</sup>. It is interesting to note that the experimental trends found also agree with the fluid model.

The model (still using  $t_{\text{acc}} = 1.3 \times \tau_{\text{laser}}$ ) also fits well with previously published measurements performed at various laser facilities as shown in Fig. 4. Taking into consideration the variety of experimental configurations, we have only selected data in similar parameter ranges in the two plots of Fig. 4. Figure 4a shows the maximum proton energy evolution versus the laser pulse duration, for two intensity ranges (circles and squares) together with the prediction of the fluid model for various intensities (lines). Comparing the laser–proton energy conversion efficiency between the same experiments and the model is more difficult, as published works do not use the same proton energy range over which the spectrum is integrated. For this reason, we have displayed in Fig. 4b the proton number for a 1 MeV bin centred at 10 MeV, for two laser pulse durations (circles and squares) together with the prediction of the fluid model using a pulse duration of 0.5 ps.

Finally, in order to validate further the use of the fluid model and to obtain more details on the acceleration mechanisms, we have

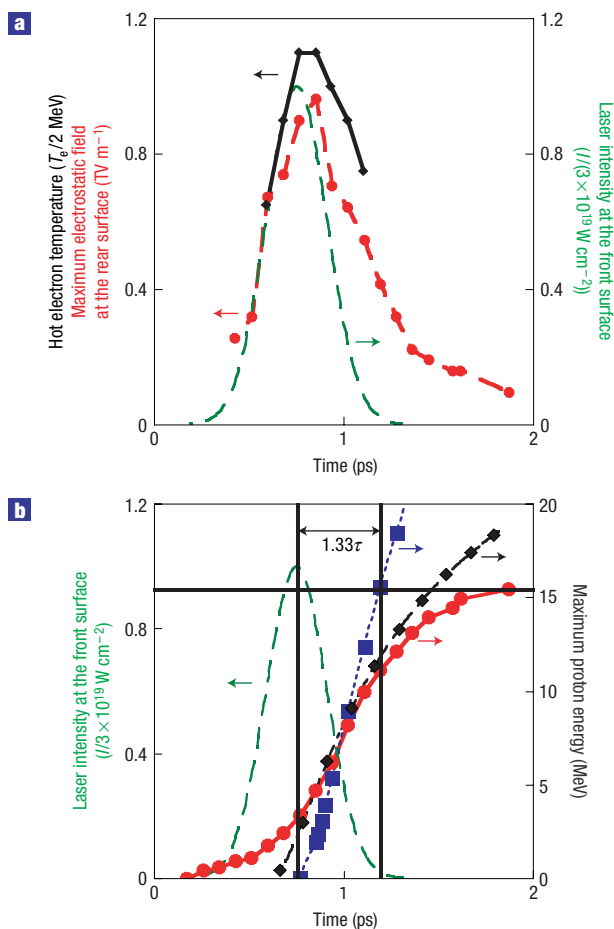


**Figure 5** Study of the evolution of the electron and proton populations during ion acceleration using PIC and fluid simulations. **a**, Temporal evolution of the maximum electrostatic field at the rear of the target (red dashed line with circles) and of the hot electron temperature (black solid line with diamonds) in two-dimensional PIC simulations. **b**, Temporal evolution of the maximum proton energy. The red solid line (with circles) corresponds to PIC simulations. The blue dotted line (with squares) corresponds to the isothermal model that starts at the maximum of the electrostatic field, with a  $1.21 \times 10^{20} \text{ cm}^{-3}$  sheath density and a hot electron temperature 2.2 MeV, as given by the PIC simulation. The black dash-dotted line (with diamonds) corresponds to a more precise fluid calculation<sup>50</sup> that takes into account the finite size of the target and the energy transfer dynamics between the electrons with a finite total energy and the ions. For both plots, the dashed green line corresponds to the laser intensity at the front surface, peaking at  $3 \times 10^{19} \text{ W cm}^{-2}$  after 750 fs. The pulse duration is 320 fs.

performed two-dimensional PIC simulations of rear-side proton acceleration with parameters similar to the experimental ones. As expected, these kinetic simulations show, as illustrated in Fig. 5a, that acceleration is far from being isothermal, and is slower than in the fluid model. Nonetheless, Fig. 5b shows that the maximum proton energy in the PIC simulation saturates at a value equal to the isothermal model prediction for a time of the order of the incident pulse duration. This numerical observation supports and explains the successful use of the isothermal model in fitting the experimental energy values. In addition, we have compared the fluid model and the PIC simulations for higher laser intensities than used in the experiments. The comparison is favourable, as can be seen in Table 1.

## APPLICATION FOR PROTON ENERGY INCREASE

Several of the applications require a significant proton energy increase compared with what has been achieved up until now. A first example is the radiography of dense objects, either static or dynamic. In the particular case of interest for inertial confinement fusion, a laminar flux of protons of 60 MeV or more would be appropriate to probe compressed pellets of 100  $\mu\text{m}$  diameter. Considering proton therapy, the production of energetic proton beams of high beam quality with lasers could provide a promising alternative to the present use of conventional accelerators. The interest of using lasers would be to take advantage of a potential significant reduction of size and cost of treatment facilities that would allow their more widespread use in the hospital environment. In order to pursue such an application, the proton energy has to be high enough to penetrate through several centimetres of tissue, that is, 60 MeV corresponding to eye tumours or to tumours in small animals for preclinical studies, and 200 MeV corresponding to the deepest zones to be treated (25 cm).

Using the fluid model as a predictive tool, we can calculate the laser parameters that would be needed to achieve, in particular, a proton beam with a maximum energy of 200 MeV. This is shown in Fig. 6 for various target thicknesses, laser pulse durations and laser spot sizes. According to Fig. 6a, there seems to be an optimum for the pulse duration in the range  $\sim 200$  fs to 1 ps in order to take full advantage of the proton acceleration time. This is longer than that previously considered in simulation feasibility studies for proton therapy, as these studies have restricted themselves to much shorter pulses<sup>10,11</sup>.

To achieve practical proton therapy treatment, there are two further requirements: (i) the delivered dose requirement; and (ii) a sufficiently small energy spread  $\Delta E/E \ll 1$  of the beam. Of course, as we have mentioned above, there is a continuous spectrum of fast protons below the maximum energy, with flux increasing rapidly as the energy decreases. However, several solutions for energy selection from this continuum have already been suggested<sup>34,35</sup>, so we chose not to repeat that material here. Considering the issue of the available proton flux per laser shot, we can use the scaling of the proton number with the laser intensity of Fig. 4b to deduce the number of protons around 200 MeV that could be produced by a laser pulse of 0.5 ps duration,  $8 \times 10^{20} \text{ W cm}^{-2}$  intensity and 3  $\mu\text{m}$  full-width at half-maximum (FWHM) focal spot irradiating a 10- $\mu\text{m}$ -thick target. In these conditions, there would be  $\sim 10^9$  particles in a  $\Delta E/E = 10^{-2}$  bin for a single laser shot. As the required particle flux for treatment is in the range of  $10^{10}$  particles per second<sup>36</sup>, a laser with a repetition rate of 10 Hz could be appropriate. Such a repetition rate is already technologically foreseeable at the required energy levels of  $\sim 100$  J (see Fig. 6a)<sup>37,38</sup>. Such high laser energies could be compressed in a short pulse using available gratings in a tiled arrangement as is now being developed for future petawatt facilities<sup>39</sup>.

## ALTERNATIVE PATHS FOR PROTON ENERGY INCREASE

There may also be alternatives to using solely solid targets as proton sources. For example, it could be ideal to have a controllable large preplasma in front of the solid. Indeed, PIC simulations have shown that a large preplasma increases the number and temperature of the accelerated electrons<sup>40</sup>. This could be achieved by using enclosures, or a flow, of controlled gas in front of the target. Another path for optimization may also be provided by the relativistic transparency regime<sup>41</sup> where simulations<sup>26</sup> show that proton acceleration should be even more efficient. In this scheme, the laser pulse interacts with the whole volume of a very thin, dense target and accelerates the whole electron population efficiently. This, however, requires ultrathin targets and therefore ultrahigh-contrast pulses, so that the peak of the pulse interacts



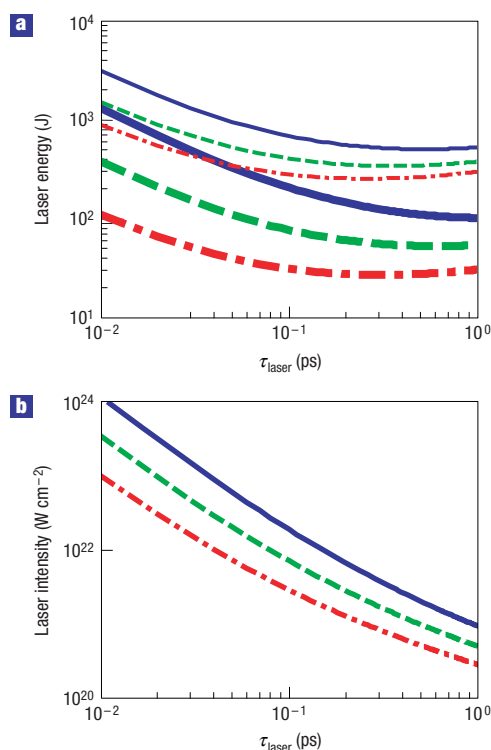


**Figure 6** Projections of required laser energy and intensity to achieve a certain proton maximum energy using the adjusted fluid model. **a**, Required laser energy in the focal spot to achieve 200 MeV as maximum proton energy for various laser pulse durations and target thicknesses (blue solid line, 25  $\mu\text{m}$ ; dashed green line, 10  $\mu\text{m}$ ; dash-dotted red line, 2  $\mu\text{m}$ ). The thinner lines are for a 10  $\mu\text{m}$  FWHM focal spot, and the thicker lines for a 3  $\mu\text{m}$  FWHM focal spot. **b**, The required laser intensity to achieve the same goal with the same parameters. The influence of the focal spot diameter is less apparent on the required intensity.

with an unperturbed target. We have conducted preliminary tests of such interactions using laser pulses with contrast enhanced by the use of two consecutive plasma mirrors<sup>42</sup>. In this configuration, we have measured  $\sim 10$  MeV maximum proton energies using 30–100-nm-thick targets and a peak laser intensity of  $5\text{--}9 \times 10^{17} \text{ W cm}^{-2}$  in a pulse duration of 350 fs. This is to be compared with the 1 MeV maximum energy protons achieved for the same pulse duration and intensity in the standard regime of rear-surface acceleration, that is, using thicker targets<sup>19</sup> (5  $\mu\text{m}$ ). However, the beam quality was somewhat lower in the transparency regime than in the standard regime of rear-surface acceleration.

## METHODS

### EXPERIMENTAL CONFIGURATION

The experiments were performed using two short-pulse lasers. These were the 100 TW laser at the Laboratoire pour l'Utilisation des Lasers Intenses (LULI), France, operating at 1.057  $\mu\text{m}$  wavelength, and the Atlas laser at the Max-Planck Institut für Quantenoptik, Germany, operating at 0.8  $\mu\text{m}$ . Both lasers operate in the well-known chirped pulse amplification mode<sup>43</sup>, where an initial short pulse of low energy is chirped temporally to allow amplification while minimizing spectral phase distortions and is then subsequently recompressed. On both facilities, dynamic wavefront correction is applied to ensure optimum and reproducible focusability at every shot. Having a constant laser focus is crucial in order to have good reproducibility of the proton beam. The focal spot FWHM are similar on both facilities: 6  $\mu\text{m}$  (LULI) and 5  $\mu\text{m}$  (Atlas) as measured directly by imaging diagnostics collecting light after

focusing. Overall, we varied  $E$  from 0.2 to 60 J,  $\tau_{\text{laser}}$  from 150 fs to 10 ps and  $I$  from  $10^{18}$  to  $6 \times 10^{19} \text{ W cm}^{-2}$ . The value of  $E$  was varied by using calibrated attenuators positioned before compression, that is, to attenuate the chirped pulse. The value of  $\tau_{\text{laser}}$  was varied by changing the distance between the gratings in the compressor chamber, and was measured by second-order autocorrelation. On both facilities, the energy that precedes the main pulse is controllable within some limits by the use of fast-switching Pockels cells. For this study, we kept the conditions constant and similar between the two lasers, that is, a maximum ASE level of  $\sim 1\text{--}5 \times 10^{12} \text{ W cm}^{-2}$ , for a duration of 1.5–2 ns as measured by a fast photodiode. At LULI, targets are irradiated either at normal incidence or at  $40^\circ$ . At Atlas,  $30^\circ$  incidence is used. We observed that the laser incidence on target had little influence on the resulting ion beam. This is most probably due to laser hole boring in the preformed plasma at high irradiance: regardless of the initial angle, all angles of incidence are present in the cavity bored into the dense plasma, and similar hot electron populations are thus produced. Detection of the proton beam is performed using radiochromic film (RCF) dosimetry media<sup>44</sup> directly exposed to the beam and Thomson parabola equipped with CR-39<sup>45</sup>. RCF provides, with a high dynamic range, continuous spatial readout of the proton fluence, in coarsely resolved steps of proton energy by means of the range–energy relationship of the stopping power. Using a stack of RCF therefore allows reconstruction of the spectrum of the proton beam. We observe that the spectra have a sharp cutoff at a maximum energy. Note that RCF is preferentially sensitive to penetrating protons, which have a large specific energy-loss and produce a high contrast image. The use of RCF to infer the proton-beam spectrum has been validated by simultaneous measurements performed using a home-made magnetic spectrometer (with a 0.6 T permanent magnet) facing the target rear side. Finally, the angularly integrated spectrum is integrated between a fixed minimal energy, here chosen to be 4 MeV, and the maximum cutoff energy. The integrated energy carried by the proton beam thus obtained is then divided by the laser initial energy to find the laser–proton energy conversion efficiency.

### NUMERICAL SIMULATIONS

In the two-dimensional PIC simulations the peak of the linearly polarized pulse reaches the target surface, at normal incidence, 750 fs after the beginning of the calculation. The target is 19  $\mu\text{m}$  thick, covered with a 19 nm layer of protons to model hydrocarbon contaminants. The initial electron temperature is 5 keV and the proton-to-electron mass ratio is 1,836. A 3  $\mu\text{m}$  linear preplasma rising from  $1.1 \times 10^{20} \text{ cm}^{-3}$  to the target density is placed in front of the target. The target density is  $2 \times 10^{22} \text{ cm}^{-3}$ . The simulation box is 134  $\mu\text{m}$  long and 24  $\mu\text{m}$  wide. The mesh size is  $\Delta x = \Delta y = 19 \text{ nm}$  and there are 35 particles per species per cell, advanced with a time step of  $4.2 \times 10^{-2} \text{ fs}$ .

Received 16 June 2005; accepted 28 November 2005; published 25 December 2005.

### References

- Clark, E. *et al.* Measurements of energetic proton transport through magnetized plasma from intense laser interactions with solids. *Phys. Rev. Lett.* **84**, 670–673 (2000).
- Snavely, R. A. *et al.* Intense high-energy proton beams from Petawatt-laser irradiation of solids. *Phys. Rev. Lett.* **85**, 2945–2948 (2000).
- Hatchett, S. *et al.* Electron, photon, and ion beams from the relativistic interaction of Petawatt laser pulses with solid targets. *Phys. Plasmas* **7**, 2076–2079 (2000).
- Gitomer, S. J. *et al.* Fast ions and hot electrons in the laser-plasma interaction. *Phys. Fluids* **29**, 2679–2688 (1986).
- Cowan, T. *et al.* Ultralow emittance, multi-MeV proton beams from a laser virtual-cathode plasma accelerator. *Phys. Rev. Lett.* **92**, 204801 (2004).
- Borghesi, M. *et al.* Multi-MeV proton source investigations in ultraintense laser-foil interactions. *Phys. Rev. Lett.* **92**, 055003 (2004).
- Fuchs, J. *et al.* Spatial uniformity of laser-accelerated ultrahigh-current MeV electron propagation in metals and insulators. *Phys. Rev. Lett.* **91**, 255002 (2003).
- Borghesi, M. *et al.* Electric field detection in laser-plasma interaction experiments via the proton imaging technique. *Phys. Plasmas* **9**, 2214 (2002).
- Patel, P. *et al.* Isochoric heating of solid-density matter with an ultrafast proton beam. *Phys. Rev. Lett.* **91**, 125004 (2003).
- Bulanov, S. V. *et al.* Oncological hadrontherapy with laser ion accelerators. *Phys. Lett. A* **299**, 240–247 (2002).
- Fourkal, E. *et al.* Particle in cell simulation of laser-accelerated proton beams for radiation therapy. *Med. Phys.* **29**, 2788–2798 (2002).
- Malka, V. *et al.* Practicability of protontherapy using compact laser systems. *Med. Phys.* **31**, 1587–1592 (2004).
- Ledingham, K., McKenna, P. & Singhal, R. Applications for nuclear phenomena generated by ultra-intense lasers. *Science* **300**, 1107–1111 (2003).
- Ledingham, K. *et al.* High power laser production of short-lived isotopes for positron emission tomography. *J. Phys. D* **37**, 2341–2345 (2004).
- McKenna, P. *et al.* Characterization of multiterawatt laser–solid interactions for proton acceleration. *Rev. Sci. Instrum.* **73**, 4176–4184 (2002).
- Zepf, M. *et al.* Fast particle generation and energy transport in laser–solid interactions. *Phys. Plasmas* **8**, 2323–2330 (2001).

17. Spencer, I. *et al.* Laser generation of proton beams for the production of short-lived positron emission radioisotopes. *Nucl. Instrum. Methods Phys. Res. B* **183**, 449–458 (2001).
18. Spencer, I. *et al.* Experimental study of proton emission from 60-fs, 200-mJ high-repetition-rate tabletop-laser pulses interacting with solid targets. *Phys. Rev. E* **67**, 046402 (2003).
19. Oishi, Y. *et al.* Dependence on laser intensity and pulse duration in proton acceleration by irradiation of ultrashort laser pulses on a Cu foil target. *Phys. Plasmas* **12**, 073102 (2005).
20. Mackinnon, A. *et al.* Enhancement of proton acceleration by hot-electron recirculation in thin foils irradiated by ultraintense laser pulses. *Phys. Rev. Lett.* **88**, 215006 (2002).
21. Kaluza, M. *et al.* Influence of the laser prepulse on proton acceleration in thin-foil experiments. *Phys. Rev. Lett.* **93**, 045003 (2004).
22. Hegelich, M. *et al.* MeV ion jets from short-pulse-laser interaction with thin foils. *Phys. Rev. Lett.* **89**, 085002 (2002).
23. Allen, M. *et al.* Direct experimental evidence of back-surface ion acceleration from laser-irradiated gold foils. *Phys. Rev. Lett.* **93**, 265004 (2004).
24. Fuchs, J. *et al.* Comparison of laser ion acceleration from the front and rear surfaces of thin foils. *Phys. Rev. Lett.* **94**, 045004 (2005).
25. Silva, L. O. *et al.* Proton shock acceleration in laser-plasma interactions. *Phys. Rev. Lett.* **92**, 015002 (2004).
26. D'Humières, E., Lefebvre, E., Gremillet, L. & Malka, V. Proton acceleration mechanisms in high-intensity laser interaction with thin foils. *Phys. Plasmas* **12**, 062704 (2005).
27. Esirkepov, T., Borghesi, M., Bulanov, S., Mourou, G. & Tajima, T. Highly efficient relativistic-ion generation in the laser-piston regime. *Phys. Rev. Lett.* **92**, 175003 (2004).
28. Mora, P. Plasma expansion into a vacuum. *Phys. Rev. Lett.* **90**, 185002 (2003).
29. Gurevich, A. V., Pariiskaya, L. V. & Pitaevskii, L. P. Self-similar motion of rarefied plasma. *Sov. Phys. JETP* **22**, 449 (1966).
30. Wilks, S. C. *et al.* Absorption of ultra-intense laser pulses. *Phys. Rev. Lett.* **69**, 1383–1386 (1992).
31. Malka, G. & Miquel, J. L. Experimental confirmation of ponderomotive-force electrons produced by an ultrarelativistic laser pulse on a solid target. *Phys. Rev. Lett.* **77**, 75–78 (1996).
32. Key, M. *et al.* Hot electron production and heating by hot electrons in fast ignitor research. *Phys. Plasmas* **5**, 1966–1972 (1998).
33. Feurer, T. *et al.* Onset of diffuse reflectivity and fast electron flux inhibition in 528-nm-laser–solid interactions at ultrahigh intensity. *Phys. Rev. E* **56**, 4608–4614 (1997).
34. Fourkal, E. *et al.* Particle selection for laser-accelerated proton therapy feasibility study. *Med. Phys.* **30**, 1660–1670 (2003).
35. Esirkepov, T. *et al.* Proposed double-layer target for the generation of high-quality laser-accelerated ion beams. *Phys. Rev. Lett.* **89**, 175003 (2002).
36. Khoroshkov, V. S. & Minakova, E. I. Proton beams in radiotherapy. *Eur. J. Phys.* **19**, 523–536 (1998).
37. Hein, J. *et al.* Diode-pumped chirped pulse amplification to the joule level. *Appl. Phys. B* **79**, 419–422 (2004).
38. Chanteloup, J. C. *et al.* Overview of the Lucia laser program: towards 100 Joules, nanosecond pulses, kW averaged power, based on Ytterbium diode pumped solid state laser. *Proc. SPIE* **5707**, 105–116 (2005).
39. Kessler, T. J. *et al.* Demonstration of coherent addition of multiple gratings for high-energy chirped-pulse-amplified lasers. *Opt. Lett.* **29**, 635–637 (2004).
40. Lefebvre, E. & Bonnaud, G. Nonlinear electron heating in ultrahigh-intensity-laser–plasma interaction. *Phys. Rev. E* **55**, 1011–1014 (1997).
41. Fuchs, J. *et al.* Transmission through highly overdense plasma slabs with a subpicosecond relativistic laser pulse. *Phys. Rev. Lett.* **80**, 2326–2329 (1998).
42. Monot, P. *et al.* High-order harmonic generation by nonlinear reflection of an intense high-contrast laser pulse on a plasma. *Opt. Lett.* **29**, 893–895 (2004).
43. Strickland, D. & Mourou, G. Compression of amplified chirped optical pulses. *Opt. Commun.* **56**, 219–221 (1985).
44. Klassen, N. V. *et al.* GafChromic MD-55: Investigated as a precision dosimeter. *Med. Phys.* **24**, 1924–1934 (1997).
45. Lefevre, H. W., Sealock, R. M. & Connolly, R. C. Response of CR-39 to 2-MeV microbeams of H, He, and Ne. *Rev. Sci. Instrum.* **53**, 1221–1227 (1982).
46. McKenna, P. *et al.* Characterization of proton and heavier ion acceleration in ultrahigh-intensity laser interactions with heated target foils. *Phys. Rev. E* **70**, 036405 (2004).
47. Murakami, Y. *et al.* Observation of proton rear emission and possible gigagauss scale magnetic fields from ultra-intense laser illuminated plastic target. *Phys. Plasmas* **8**, 4138–4143 (2001).
48. Maksimchuk, A. *et al.* High-energy ion generation by short laser pulses. *Plasma Phys. Rep.* **30**, 473–495 (2004).
49. Fujii, T. *et al.* MeV-order proton and carbon ion acceleration by irradiation of 60 fs TW laser pulses on thin copper tape. *Appl. Phys. Lett.* **83**, 1524–1526 (2003).
50. Mora, P. Thin foil expansion into a vacuum. *Phys. Rev. E* **72**, 056401 (2005).

### Acknowledgements

We acknowledge the expert support of the LULI and Atlas laser teams and useful discussion with T. Cowan, A. Kemp and Y. Sentoku. This work was supported by DAAD, grant E1127 from Région Ile-de-France, the EU programme HPRI CT 1999-0052, and UNR grant DE-FC08-01NV14050. Correspondence and requests for materials should be addressed to J.F.

### Competing financial interests

The authors declare that they have no competing financial interests.

Reprints and permission information is available online at <http://npg.nature.com/reprintsandpermissions/>